Impact of water uptake and mixing state on submicron particles deposition in the human respiratory tract (HRT): Based on explicit hygroscopicity measurements at HRT-like conditions

Ruiqi Man[1], Zhijun Wu[1,2], Taomou Zong[1], Aristeidis Voliotis[3,4], Johannes Größ[5], Dominik van Pinxteren[5], Limin Zeng[1], Hartmut Herrmann[5], Alfred Wiedensohler[5], Min Hu[1]

[1]State Key Joint Laboratory of Environmental Simulation and Pollution Control, College of Environmental Sciences and Engineering, Peking University, 100871, Beijing, China

[2]Collaborative Innovation Center of Atmospheric Environment and Equipment Technology, Nanjing University of Information Science and Technology, 210044, Nanjing, China

[3]National Centre for Atmospheric Science, Department of Earth and Environmental Science, School of Natural Sciences, The University of Manchester, Oxford Road, M13 9PL, Manchester, UK

[4]Centre for Atmospheric Science, Department of Earth and Environmental Science, School of Natural Sciences, The University of Manchester, Oxford Road, M13 9PL, Manchester, UK

[5]Leibniz Institute for Tropospheric Research, 04318, Leipzig, Germany

Correspondence to: Zhijun Wu (zhijunwu@pku.edu.cn)

Abstract. The particle hygroscopicity plays a key role in determining the particle deposition in the human respiratory tract (HRT). In this study, the effects of hygroscopicity and mixing state on regional and total deposition doses for children, adults, and elderly were quantified using the Multiple-Path Particle Dosimetry model based on the size-resolved particle hygroscopicity measurements at HRT-like conditions (relative humidity = 98%) performed in the North China Plain. The measured particle population with an external mixing state was dominated by hygroscopic particles (number fraction = (91.5 ± 5.7)%, mean ± standard deviation (SD), the same below). Particle hygroscopic growth in the HRT led to a reduction by around 24% in the total doses of submicron particles for all age groups. Such reduction was mainly caused by the growth of hygroscopic particles and was more pronounced in the pulmonary and tracheobronchial regions. Regardless of hygroscopicity, the elderly group had the highest total dose among the three age groups. With 270 nm in diameter as the boundary, the total deposition doses of particles smaller than this diameter were overestimated and those of larger particles were underestimated assuming no particle hygroscopic growth in the HRT. From the perspective of the daily variation, the deposition rates of hygroscopic particles with an average of (2.88 ± 0.81) × 10^9 #/h (SD =

32 ~~8.10 × 10⁸ #/h)~~ during the daytime were larger than those $((2.32 ~~-~~ \pm 0.81) \times 10^9 ~~) \pm (2.41 \times 10^8)~~$ #/h) at

33 night. On the contrary, hydrophobic particles interpreted as freshly emitted soot and primary organic

34 aerosols exhibited higher deposition rates at nighttime $((3.39 \pm 1.34) \times 10^8$ #/h) than those in the day

35 $((2.58 \pm 0.76) \times 10^8 ~~) \pm (7.60 \times 10^7)~~$ #/h). The traffic emissions during the rush hours enhanced the

36 deposition rate of hydrophobic particles. This work provides a more explicit assessment of the impact of

37 hygroscopicity and mixing state on the deposition pattern of submicron particles in the HRT.

38 **Keywords:** hygroscopicity; mixing state; HH-TDMA; lung deposition; MPPD

1 Introduction

Toxicological and epidemiological studies showed that ambient particles can result in the declining life expectancy and rising premature mortality were both closely related to ambient particles (Chen et al., 2013; Correia et al., 2013; Pope and Dockery, 2013; Ching and Kajino, 2018; Dockery et al., 1993; Pope et al., 2009). Compared with coarse particles, submicron particles (i.e., particles with diameter ≤ 1 μm) have smaller sizes and larger specific surface areas, which tend to carry more toxic and harmful components and reach deeper into the human respiratory tract (HRT) (Oberdorster, 2001). Inhaled particles deposit along the HRT mainly by diffusion, sedimentation, impaction, and interception (Wang et al., 2018a). The major deposition mechanism depends on the particle size and specific deposition location (Varghese and Gangamma, 2009). Unlike ambient environments, conditions in the HRT are warm and humid, where the relative humidity (RH) can be as high as 99.5% (Hussein et al., 2013). The unique environment can alter the chemical and physical characteristics of inhaled particles, leading to variations in particle deposition distributions and doses. To accurately quantify the deposition pattern of submicron particles in the HRT, it is therefore critical to account for such potential transformations and characterize inhaled particle properties in the HRT.

Due to experimental limitations of measuring inhaled particle number size distributions (PNSDs), regional doses in the HRT are typically estimated by means of mathematical models (Hofmann, 2011). The most widely used dosimetry models are the International Commission on Radiological Protection (ICRP, 1994) model and the Multiple-Path Particle Dosimetry (MPPD) model (Asgharian et al., 2001). Estimating the particle deposition fraction (DF) in these models is based on aerosol properties as well as individual's physiological parameters. These available dosimetry models, however, fail to incorporate some critical particle characteristics, especially the hygroscopicity (Ferron, 1977), which may cause variations in the particle size and therefore affect the deposition efficiency and pattern of particles in different lung regions.

To date, many studies have assessed the effects of hygroscopicity on ambient particle deposition in the HRT based on assumed values of the hygroscopic parameter (Kappa, κ) representing non-hygroscopic, nearly hydrophobic, and hygroscopic particles (Voliotis and Samara, 2018) or estimations using models from κ of each chemical composition (Chalvatzaki and Lazaridis, 2018; Ching and Kajino, 2018; Haddrell et al., 2015; Hussein et al., 2013; Martonen and Schroeter, 2003; Rajaraman et al., 2020; Vu et al., 2015; Vu et al., 2018; Xu et al., 2021; Londahl et al., 2007). However, it is well-known that continental aerosols typically show an external mixing state and size-dependent hygroscopicity (Zong et al., 2021). Thus, in order to capture the real features of ambient particles' hygroscopic growth in the HRT, direct particle hygroscopic growth measurements(Cuevas Robles et al., 2021; Farkas et al., 2022; Kristensson et al., 2013; Londahl et al., 2009; Vu et al., 2015; Youn et al., 2016) are a matter of necessity.

Hygroscopicity measurements of ambient aerosols under subsaturated conditions are generallymainly conducted by Humidity Tandem Differential Mobility Analyzer (H-TDMA) (Farkas et al., 2022; Kristensson et al., 2013; Londahl et al., 2009) or Differential Aerosol Sizing and Hygroscopicity Spectrometer Probe (DASH-SP) (Cuevas-Robles et al., 2021; Youn et al., 2016). For example, Farkas et al. (2022) modelled DFs of aerosol particles with four different diameters and studied in their dry state and after their hygroscopic growth at RH = 90% using a H-TDMA (Farkas et al., 2022).

79   Youn et al. (2016) examined size-resolved hygroscopicity data by DASH-SP for particles sampled near

80   mining and smelting operations to study the effects of particles' hygroscopic growth on the HRT

81   deposition of toxic contaminants ~~(Youn et al., 2016)~~. Most of such studies used hygroscopicity data

82   measured at considerably lower RH conditions opposed to those occurring in the HRT (85%-90% vs. ≈

83   99.5%) (Vu et al., 2015; Swietlicki et al., 2008). It was further assumed that κ was independent of RH

84   ~~under~~on the premise ~~of~~ that the ~~ideal solution~~ effective molar volume of the solute does not vary with

85   RH. However, the presence of surface active, slightly soluble substances, and the co-condensation of

86   semi-volatile soluble organic compounds can result in the humidity-dependent characteristic of κ (Wu et

87   al., 2013; Wex et al., 2009; Topping and Mcfiggans, 2012). For instance, Liu et al. (2018) showed that κ

88   could vary from about 0.1 at RH < 20% to less than 0.05 when RH ≈ 90% due to the non-ideal mixing

89   of water with hydrophobic and hydrophilic organic components ~~(Liu et al., 2018)~~. Therefore, an explicit

90   hygroscopicity measurements at HRT-like conditions will make the deposition estimation more accurate.

91   In this study, the size-resolved particle hygroscopicity derived from a high humidity tandem

92   differential mobility analyzer (HH-TDMA) at HRT-like conditions (RH = 98%) was used to quantify the

93   effects of both hygroscopicity and external mixing state on the particle deposition in the HRT using the

94   MPPD model. The deposition doses of submicron particles were calculated in the head, tracheobronchial

95   (TB), and pulmonary (P) regions in the HRT for different age groups. Further, the diurnal variations of

96   deposition rates of hygroscopic and hydrophobic particles were also calculated to provide an insight into

97   the particle deposition linked to human activities.

98   **2 Materials and Methods**

99   **2.1 The Sampling Site and Instruments**

100   The field campaign was conducted from June 8 to July 6 in 2014 at an ecological park in the rural

101   area of Wangdu County (38.666ºN, 115.210ºE) in the North China Plain. The surroundings were wheat

102   fields without significant industry emissions. A detailed description of the sampling site can be found in

103   our previous study (Wu et al., 2017b). In brief, a HH-TDMA and a twin differential mobility particle

104   sizer (TDMPS) were employed to measure the hygroscopic growth factor (HGF) of specific size particles

105   at RH = 98% and the size-resolved PNSDs of particles ranging from 3 to 800 nm respectively. Besides,

106   NO and CO was monitored by a NOx chemiluminescence analyzer (42i-TLE, Thermo Scientific) and a

107   Trace Level Carbon Monoxide Analyzer (48iQ, Thermo Scientific), respectively (Chen et al., 2020). The

108   BC mass concentrations were measured by a Multi-Angle Absorption Photometer (MAAP Model 5012,

109   Thermo, Inc.) (Wang et al., 2019). The OH radical was measured by a Laser-induced fluorescence (LIF)

110   (Tan et al., 2020).

111   **2.2 Particle Hygroscopic Growth Measurement**

The HH-TDMA was designed to measure the aerosol hygroscopic growth at high RH (90% - 98%), using the technique of a temperature-controlled water bath, which is able to hold the RH of aerosols and sheath flow stable for RH > 90% (Hennig et al., 2005). The RH in the second differential mobility analyzers (DMA) reached an absolute accuracy of ±1.2% for 98% and a long-term stability of ± 0.1-0.4% of set point values (Hennig et al., 2005). More detailed information regarding the HH-TDMA system was provided by Bian et al. (2014) and Wu et al. (2017a). The HGF was defined as the ratio of the wet particle diameter at a given RH ($D_{P,wet}$) to the dry particle diameter for RH < 10% ($D_{P,dry}$):

$$HGF = \frac{D_{P,wet}}{D_{P,dry}}, \tag{1}$$

The TDMAinv method developed by Gysel et al. (2009) was used to invert hygroscopicity data of settled diameter particles (30, 50, 100, 150, 200, and 250 nm) to HGFs of size-resolved particles and hygroscopic growth factor probability distribution function (GF-PDF) at RH = 98% (Gysel et al., 2009). The HGF was then converted into the hygroscopic parameter (κ) according to the κ-Köhler theory (Petters and Kreidenweis, 2007):

$$\kappa = (HGF^3 - 1)(\frac{\exp\left(\frac{A}{D_{P,dry} \cdot HGF}\right)}{RH} - 1), \tag{2}$$

$$A = \frac{4\sigma_{s/a}M_w}{RT\rho_w}, \tag{3}$$

where HGF and $D_{P,dry}$ are the hygroscopic growth factor measured at 98% RH by HH-TDMA and the dry particle diameter respectively, $\sigma_{s/a}$ is the droplet surface tension (assumed to be that of pure water, $\sigma_{s/a} = 0.0728\,\text{N m}^{-2}$), M_w is the molecular weight of water, ρ_w is the density of liquid water, R is the universal gas constant, and T is the absolute temperature.

The head region, or upper respiratory tract, includes the nasal cavities, the pharynx, and the larynx. In this study, the wet diameter of aerosols above the larynx was assumed to be equilibrated with ~~the~~ ambient air conditions (Ching and Kajino, 2018), therefore set to the average value during the sampling period (T = 26 ℃, RH = 60%). The TB and P regions belong to the lower respiratory tract which were saturated with water vapor, and the temperature and RH inside were 37 ℃ and 99.5%, respectively (Vu et al., 2015). The wet particle diameter in the HRT was estimated by using the variant of Eq (2). Detailed information can be found in Farkas et al. (2022). It should be noticed that the inhaled particle was assumed to reach the equilibrium size immediately once particles enter into the HRT in this study. However, the hygroscopic growth rate of particles depends on the particle size, hygroscopicity, the ambient environment conditions (such as RH and temperature), and the residence time in the body (Ching and Kajino, 2018). A previous study pointed out that particles with $D_p = 100$ nm can reach the equilibrium

139 size in a few seconds, while the equilibration timescale of particles with D_p > 1 μm turn to minutes (Ching

140 and Kajino, 2018).

2.3 Total, Hygroscopic, and Hydrophobic Particle Number Size Distributions

142 The TDMPS includes two Hauke-type ~~differential mobility analyzers (~~DMA~~)~~ that have different

143 effective center rod lengths which measure aerosol particles of 20 - 800 nm and 3 - 20 nm, respectively.

144 The two condensation particle counters (CPC) count particles downstream of DMAs. Combining the

145 counts from the two CPCs, the TDMPS can measure the PNSD of particles from 3 ~~–~~to 800 nm (electrical

146 mobility diameter). The instrument principle and structure of TDMPS can be found in Birmili et al.

147 (1999) and Wiedensohler et al. (2012). ~~In this study,~~ To match the particle size range in the MPPD model,

148 the electrical mobility diameter~~s~~ was converted to aerodynamic diameter~~s~~ by Eq (4) (Khlystov et al.,

149 2004):

$$d_a = d_m \sqrt{\chi \times \frac{\rho \times C_{c(dm)}}{C_{c(da)}}} \tag{4}$$

150 where d_a and d_m is the particle aerodynamic diameter (nm) and electrical mobility diameter (nm),

151 respectively. ρ is the particle density (1.5 g cm^{-3} in this study (Hu et al., 2012)). χ is the shape factor.

152 C_c is the Cunningham slip correction factor for a certain diameter. Similar to other studies, the shape

153 factor χ is assumed as 1 and C_c is neglected in the calculation (Khlystov et al., 2004; Hu et al., 2012).

154 Therefore, the electrical mobility diameter (in the range of 10.3 - 756.6 nm) was converted to the

155 aerodynamic diameter (in the range of 12.6 - 926.6 nm).

156 Taking particle mixing state into account, the particle population can be categorized into

157 hygroscopic and hydrophobic groups according to HGFs measured at RH = 98% by HH-TDMA.

158 Particles with HGF < 1.2 were regarded as hydrophobic particles whereas those with HGF ≥ 1.2 were

159 regarded as hygroscopic particles (Wang et al., 2018b; Zong et al., 2021). The hydrophobic particles in

160 urban environments have ~~previously~~ been interpreted as originating from freshly emitted soot and vehicle

161 exhaust ~~particles~~, while the hygroscopic particles have been regarded ~~as to~~more ~~processed and long-~~

162 ~~range transported~~ experience long-distance transport (Swietlicki et al., 2008; Baltensperger, 2002). To

163 obtain the PNSDs for both groups, the total PNSD measured by TDMPS were scaled by the number

164 fractions (NF) of hydrophobic and hygroscopic particles. With HGF = 1.2 as the cut-off point, the GF-

165 PDF for each selected size was divided into the hydrophobic and hygroscopic modes. The calculation

166 methods of the HGF and NF of each mode were detailed in Zong et al. (2021). The NFs of size-resolved

167 particles within the measuring range of the TDMPS were calculated by linear interpolation methods,

168 while those of particles out of the range were equal to the closest known NF.

169 **2.4 Particle Dose Estimation**

170 The MPPD model (version 3.04) was used to estimate the deposition of particles in the HRT (MPPD:

171 Multiple-Path Particle Dosimetry Model, 2022), since it fits with the measured data better than the ICRP

172 model (Londahl et al., 2007). This model calculates deposition and clearance of monodisperse and

173 polydisperse aerosols in the size range of 1 nm - 100 μm in the respiratory tracts of laboratory animals,

174 human adults, and children. Within each airway, the deposition is calculated using theoretically derived

175 efficiencies for deposition by diffusion, sedimentation, impaction, and interception within the airway or

176 airway bifurcation (MPPD: Multiple-Path Particle Dosimetry Model, 2022). The model requires the

177 following parameters as input: (1) airway morphometry parameters (airway morphometry model,

178 functional residual capacity (FRC), and the upper respiratory tract (URT) volume); (2) particle properties

179 (density, diameter); (3) exposure scenario (breathing frequency (BF), tidal volume (TV)); and (4)

180 deposition/clearance.

181 In this study, the stochastic model (60th percentile) was chosen, which is closer to the realistic

182 structure of human lungs (Voliotis and Samara, 2018; Li et al., 2016; Asgharian et al., 2001; Wang et al.,

183 2021; Lyu et al., 2018; Avino et al., 2018; Manigrasso et al., 2015). The particle diameter range was set

184 as 0.01 - 10.0 μm. Particle density was taken as 1.5 g/cm^3 according to a previous study in Beijing (Hu

185 et al., 2012). In order to obtain the deposition pattern of different age groups, the population was divided

186 into three groups on the basis of their age: children (7 - 12 years old), adults (18 - 26 years old), and the

187 elderly (> 59 years old). Then, the particle deposition was estimated based on Chinese localized

188 physiological parameters (Table 1). These values were considered for an exposure scenario for resting

189 (e.g., sitting) and nasal breathing. All the model simulations were conducted based on this exposure

190 scenario using the male physiological parameters, as corresponding data for females were not available.

191 Elsewhere it was shown that males received higher doses compared to females in all age classes due to

192 the different physiological parameters (e.g., higher TV and FRC) (Voliotis and Samara, 2018), hence

193 similar behavior would have been expected here. Similarly, different exposure scenarios (e.g. sleeping,

194 exercising, walking, etc) can result in different dose estimations and are not discussed here. For instance,

previous studies found that the exercise level had great impact on the minute ventilation and led to the increasing deposition dose (Londahl et al., 2007). All the other model input parameters were set as default. It should be noted that any clearance mechanisms were not considered in this study, hence our results show the upper limit of exposure.

Table 1 Physiological and breathing parameters for three age groups

Age Groups[a]	FRC/mL	Height[e]/cm	URT Volume[f]/mL	TV[e]/ mL	BF[e]/ min⁻¹	Exposure Time/ min day⁻¹
Children	1330[b,c]	139.3	21.91	630	22	96[g]
Adults	3338[d]	158.5	36.31	730	18	253[h]
Elderly	3259[d]	166.9	34.01	760	18	241[h]

[a] Base on the available data, age groups here refer to males.

[b] Due to the lack of data, the FRC value of children is not a Chinese localization parameter.

[c] Stocks and Quanjer, 1995

[d] Cao, 2009

[e] Zhu, 2006

[f] Hart et al., 1963

[g] Duan, 2016

[h] Duan et al., 2014

The DF is the ratio of the mass/number/surface area of the deposited particles to that of inhaled particles in a given region. The DFs of hygroscopic and hydrophobic particles with considering hygroscopicity (hereinafter referred to as "wet particles") were obtained based on the DFs of particles without considering hygroscopicity (hereinafter referred to as "dry particles"). More specifically, it is considered that the DF of wet particles with D_p after hygroscopic growth was equal to that of dry particles with the same diameter (D_p). Therefore, the DF curve of wet particles corresponds to shifting the particle size range of the DF curve of dry particles to the right. The daily particle number doses and deposition rates for size-resolved particles in a specific region were calculated as follows (Voliotis and Samara, 2018),

$$Dose_i = DF_i \times PNC_i \times TV \times BF \times t \tag{5}$$

$$Rate_i = DF_i \times PNC_i \times TV \times BF \tag{6}$$

where $Dose_i$ is the deposition dose of ith size particle (#particles/day), $Rate_i$ is the deposition rate of ith size particle (#particles/h), DF_i is the deposition fraction of ith size channel in a specific region, PNC_i is the particle number concentration (#/cm³) corresponding to the ith size channel, TV is the tidal volume (mL), BF is the breathing frequency (min⁻¹), and t is the exposure time in ambient air (min/day). The deposition dose of a specific region was calculated by adding together doses of size-resolved particles, and the total dose was the sum of three regional doses. The dose without considering hygroscopicity was calculated on the basis of the dry PNSD. The dose considering hygroscopicity was the sum of particle doses of hygroscopic and hydrophobic groups, which was respectively calculated by the PNSD of two groups.

3 Results and Discussion

3.1 Particle Number Size Distributions in the human respiratory tract

As described in Sect. 2.3, particles were categorized into hygroscopic and hydrophobic groups at RH = 98% according to their hygroscopicity. The hygroscopicity of size-resolved particles measured by HH-TDMA during the sampling period was displayed in Table S1. Figure 1 showed the average ambient PNSD under dry conditions (RH < 30%) over the entire field campaign and those of hygroscopic and hydrophobic particles in the HRT. The wet diameters of hydrophobic and hygroscopic particles in the HRT were shown in Table S2. The average particle number concentrations (PNCs) of hygroscopic and hydrophobic particles were (1.76 ± 1.64) × 10^4 (mean ± standard deviation (SD), the same below) and (1.70 ± 3.14) × 10^3 #/cm^3, respectively. The hygroscopic particles accounted for an average of (91.5 ± 5.7) % of the total PNC and dominated the measured aerosol population. The PNSDs of ambient aerosols during the daytime and nighttime were shown in Figure S1.
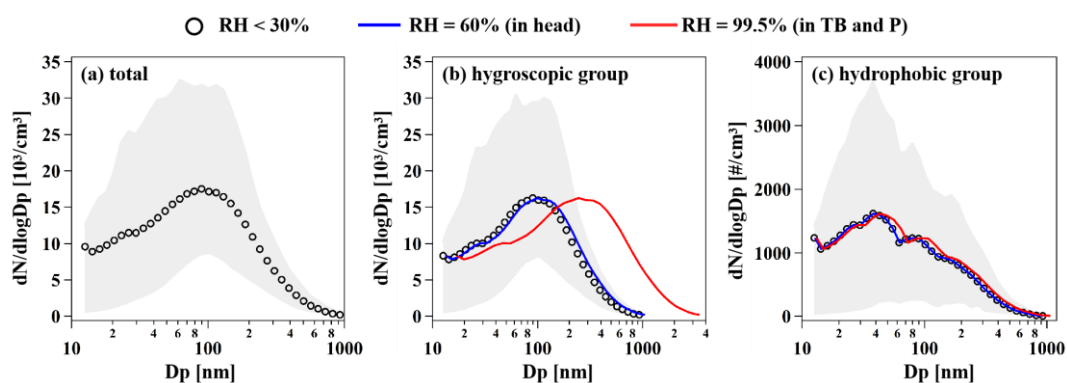
Figure 1. (a) The average particle number size distribution (PNSD) measured by TDMPS during the sampling period. The average PNSDs of the (b) hygroscopic and (c) hydrophobic groups in the human respiratory tract at different relative humidities (RHs). The ~~grey~~black ~~dots~~markers, blue lines, and red lines represent PNSDs under dry conditions (RH < 30%), in the head (RH = 60%), and in the TB and P (RH = 99.5%), respectively. The upper and lower edges of the grey area represent the 90th and 10th quantiles of PNSDs, respectively.

As shown in Figure 1(b), the hygroscopic particles grew slightly in the head (the blue line), while they had a remarkable growth in the TB and P regions (the red line) attributed to high humidity conditions and water uptake. Particularly, the diameter of hygroscopic particles corresponding to the maximum PNC shifted from about 90 nm to 250 nm. As expected, no obvious size growth of hydrophobic particles took place in the three regions in the HRT, and the peak appeared at $D_p \approx 40$ nm (Figure 1(c)).

3.2 Regional and Total Deposition Fractions

Taking the adults group as an example, size-resolved regional and total DFs of particles under dry conditions (black dots), and hydrophobic (blue dots) and hygroscopic (red dots) particles in humid environments were shown in Figure 2. The size-resolved DFs for the children and the elderly groups were shown in Figure S2-S3.
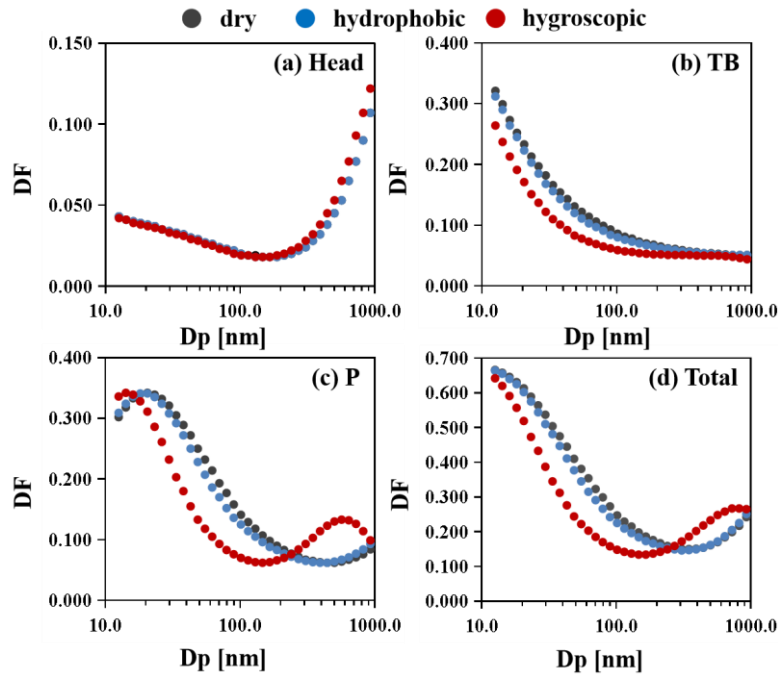
Figure 2. Size-resolved (a) head, (b) TB, (c) P, and (d) total deposition fractions (DFs) of particles under dry conditions (i.e., without considering hygroscopicity), and hydrophobic and hygroscopic particles in humid environments (i.e., considering hygroscopicity) for the adults group. For clarity, the abscissa of Figure 2 refers to the dry diameter of particles. The black, blue, and red dots represent dry, hydrophobic, and hygroscopic particles, respectively. In Figure 2(a), the black dots representing DFs under dry conditions is hidden behind the blue dots representing DFs of hydrophobic particles, because these two sets of DFs are close to each other.

As shown in Figure 2(a), there was no significant difference between head DFs whether hygroscopicity was considered or not, because the conditions within the upper respiratory tract were in balance with the surrounding environment (Ching and Kajino, 2018). With the increasing D_p, the head DFs decreased at first and reached the minimum at around 150 nm, then increased sharply, which is similar to the trend of the head DF curve using MPPD by Youn et al. (2016) ~~(Youn et al., 2016)~~.

In the TB, the DF declined monotonically associated with the increasing particle diameter, and tended to plateau for particles with $D_p > \sim 100$ nm (Figure 2(b)), which is consistent with the results of previous studies (Youn et al., 2016; Hussein et al., 2019; Varghese and Gangamma, 2009). If hygroscopicity was not taken into consideration, DFs of submicron particles were overestimated for both groups (i.e., the blue dots for hydrophobic particles and the red dots for hygroscopic particles). Using the percentage of the difference between DFs in two cases (i.e., considering hygroscopicity or not) and the DF without considering hygroscopicity as a weight, tracheobronchial DFs of hydrophobic particles were overestimated by less than 9.7%, while, 23.0% on average for hygroscopic particles. For example, the DF of particles with dry diameters at around 50 nm was 0.131 without considering hygroscopicity, and it shifted to 0.120 for hydrophobic and 0.083 for hygroscopic particles considering hygroscopicity, with the differences of 8.4% and 36.6%.

Compared with size-resolved DFs of particles under dry conditions (the black dots in Figure 2(c)), the DFs of hydrophobic (the blue dots) and hygroscopic (the red dots) particles in the P region were overestimated in the range of 20 - 500 nm and 20 - 250 nm respectively, and those of particles outside

the above diameter ranges were underestimated. The DFs of hydrophobic and hygroscopic particles were respectively overestimated (underestimated) by up to 14.1% (10.7%) and 53.1% (109.7%). Similarly, taking particles with a dry particle diameter of 50 nm as an example, the DF in the P was 0.250 without considering hygroscopicity, while it reduced to 0.133 (0.228) for hygroscopic (hydrophobic) particles considering hygroscopicity. Besides, resembled with the results of Youn et al. (2016) and Varghese et al. (2009), there was only one peak at the DF curve of the P region in the submicron range without considering hygroscopicity (black dots). Considering hygroscopicity, another peak of larger hygroscopic particles (~ 800 nm) appeared. It indicates that particle hygroscopicity enables more submicron particles with relatively large diameters to deposit in the deepest parts of the lung. It should be noted that the particle density would change during hygroscopic growth, which was not considered in the calculation due to the lack of the measurement of the particle density. The sensitivity analysis of the particle density on the regional DFs was shown in Figure S4.

In Figure 2(d), the total DFs of hydrophobic particles (the blue dots) had a similar trend as those of dry particles due to regional DFs mentioned above. For the hygroscopic group (the red dots), with D_p = 270 nm as the boundary, DFs of smaller particles were overestimated by 27.6% on average, while those of larger particles were underestimated by 28.6% on average. When considering hygroscopicity, submicron particles undergo hygroscopic growth by water uptake, and particle sizes increase as a whole (Figure 1(b) and (c)). For small particles dominated by diffusion, as D_p increasing, Brownian motion intensity decreased, and the diffusion deposition decreased accordingly. For large particles dominated by interception and inertial impaction, these two efficiencies increased with the particle size. Therefore, the corresponding particle deposition increased. This result is consistent with the previous study using the ICRP model which concluded that the deposition of particles with D_p < 200 nm was overestimated without considering water uptake (Vu et al., 2015). Additionally, the trend of the total DFs in both cases in this study is similar to the experimental data of breathing NaCl with/without hygroscopicity through noses (Chalvatzaki and Lazaridis, 2018). In general, hygroscopicity has a significant effect on regional DFs of hygroscopic particles in the TB and P regions. While, no obvious variation occurred in the DFs of two groups in the head or those of hydrophodic particles in the TB and P.

3.3 Regional and Total Deposition Doses for Different Age Groups

Regional (head, TB, and P) and total deposition number doses with/without considering hygroscopicity were calculated for children (a), adults (b), and the elderly (c) in Figure 3. Specific values of deposition doses of hydrophobic and hygroscopic particles in two cases can be found in Table S1 S3 S3-S5. Hussein et al. (2013) (Hussein et al., 2013) found that the deposited dose calculations in the other age groups (the elderly and teens) were in the same order of magnitudes as that of adults. This is also true in our results. In both cases, the elderly group had the highest total deposition dose among the three groups, followed by adults and children. While, Voliotis et al. (2018) concluded that adults received the highest doses among all age groups, which may be caused by different physiological parameter values, such as TV. In each group, the contribution of the P region to the total dose was the greatest (> ~ 55%), which was similar to the published conclusions (Voliotis and Samara, 2018; Hussein et al., 2013; Manigrasso et al., 2017; Li et al., 2016). Taking hygroscopicity into consideration, total deposition doses

significantly reduced by about a quarter (24.0% - 24.1%) for all age groups. The greatest reduction took place in doses in the P region (25.9% - 26.3%), followed by doses in the TB (24.2% - 26.1%). Head deposition had only minor variations (-0.9% - +0.5%) in both cases.
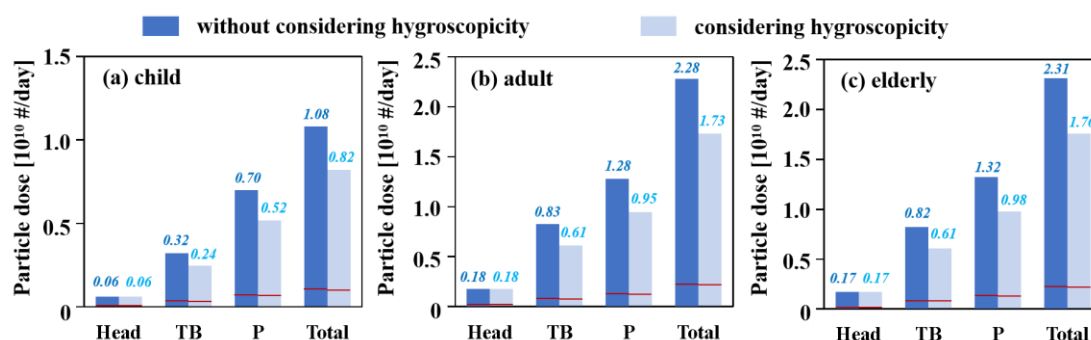
Figure 3. Regional and total deposition doses for (a) children, (b) adults, and (c) the elderly with/without considering particle hygroscopicity. The dark blue columns represent doses without considering hygroscopicity. The light blue columns represent doses considering hygroscopicity. The red lines on the column represent the division of doses of hygroscopic (above the red line) and hydrophobic particles (below the red line). Numbers above each column mean the corresponding particle doses with a unit of 10^{10} ~~particles#~~/day.

In both cases, adults (Figure 3(b)) and the elderly (Figure 3(c)) groups received similar regional and total doses. In contrast, children had the minimum total dose (Figure 3(a)), which was around half (47.4% on average) to that for adults. As shown in Eq (4), the exposure time is an important parameter for deposition dose calculations. The exposure time of the adults and the elderly groups was more than twice than that of children (Table 1), which resulted in the greater deposition dose for the former two groups. However, due to the availability of data, only localized physiological parameters for resting were obtained. People may rest, take light exercise, or take heavy exercise in the exposure time. Since the higher exercise level contributes to the greater particle deposition (Londahl et al., 2007), the actual deposition dose may be underestimated. Therefore, to remove the impact of the exposure time, the regional and total deposition rates for three age groups were also calculated and shown in Figure S5. The proportion of pulmonary deposition in total doses for children was up to 62.9% considering hygroscopicity. By comparison, it accounted for 54.6% and 55.7% for adults and the elderly groups, respectively. This indicates that particles inhaled by children are more likely to deposit in their pulmonary regions, which is in accordance with the results of previous studies (Voliotis and Samara, 2018; Voliotis et al., 2021).

As shown by the red lines in Figure 3, the contribution of hydrophobic particles to total deposition doses was about 10.0% for all age groups, while it increased to 12.5% after considering hygroscopicity. Hydrophobic particles were assumed to originate from freshly emitted soot and exhaust particles (Swietlicki et al., 2008; Baltensperger, 2002), which are composed of species that do great harm to human health, such as black carbon (BC) (Highwood and Kinnersley, 2006), primary organic aerosols (Mauderly and Chow, 2008), and polycyclic aromatic hydrocarbons (Kim et al., 2013; Haritash and Kaushik, 2009). Therefore, we need to pay attention to the deposition effects of hydrophobic particles.

The adults' regional and total deposition doses of size-resolved particles with/without considering

hygroscopicity were shown in Figure 4. The effects of hygroscopicity in particle doses in the head (Figure 4(a)) are insignificant, because the RH in the upper respiratory tract was close to that under dry conditions. Regional doses in the TB decreased due to particle hygroscopic growth (Figure 4(b)), and the greatest reduction (~ 33%) appeared between 40 and 80 nm in diameter. Similarly, particle hygroscopicity considerably decreased deposition doses (up to 50.3%) in the P region for particle sizes between 20 and 240 nm (Figure 4(c)). Inversely, particle doses increased (up to 102.6%) in the P region for diameters less than 20 nm and above 240 nm due to hygroscopic growth. As a result, the total deposition dose, as shown in Figure 4(d), was overestimated for particles smaller than around 270 nm with a maximum of 40.8% without considering hygroscopicity. The deposition doses of particles larger than this diameter were underestimated and the maximum was 43.0%.
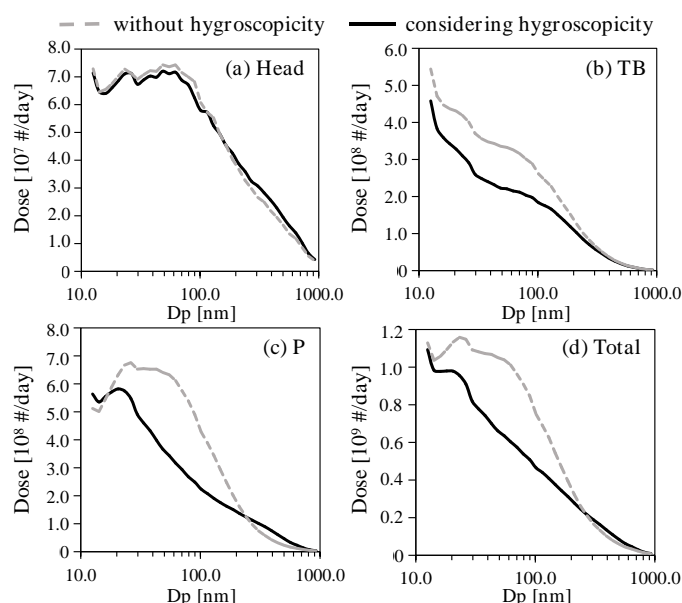
Figure 4. (a) Head, (b) TB, (c) P, and (d) total deposition doses of size-resolved particles for the adults group with/without considering hygroscopicity. For clarity, the abscissa of Figure 4 refers to the dry diameter of particles. The grey dashed line represents doses without considering hygroscopicity. The black solid line represents doses considering hygroscopicity.

3.4 Deposition Rates of Hygroscopic and Hydrophobic Particles

In order to link human daily activities to the particulate matter deposition, the diurnal variations of deposition rates of hygroscopic and hydrophobic particles considering hygroscopicity for the adults group averaged over the entire field campaign were investigated and displayed in Figure 5. Additionally, the average concentrations of NO, CO, BC, and OH radical were also given in Figure 5. By comparison, the diurnal variations of the deposition rates of hygroscopic and hydrophobic particles without considering hygroscopicity were displayed in Figure S6. No matter which time was considered during a day, the deposition rate of hygroscopic particles ($(3.60 \pm 6.68) \times 10^9$ #/h) in the HRT was nearly one magnitude higher than that of hydrophobic particles ($(5.15 \pm 14.4) \times 10^8$ #/h).
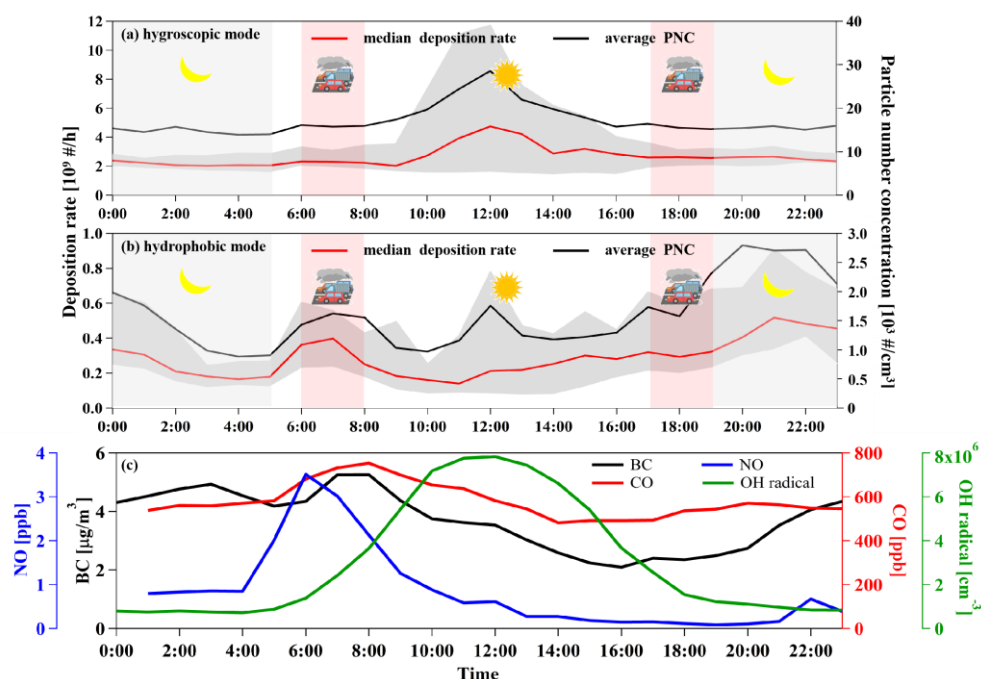
Figure 5. The diurnal variations of deposition rates considering hygroscopicity and particle number concentrations (PNCs) of (a) hygroscopic and (b) hydrophobic particles for the adults group. The red lines represent the median deposition rate. The upper and lower edges of the grey area represent the 75th and 25th quantiles of deposition rates, respectively. The black lines represent the average PNC. (c) The diurnal variations of the average concentrations of NO, CO, BC, and OH radical during the sampling period. The blue, red, black, and green lines represent NO, CO, BC, and OH radical, respectively.

The deposition rate of hygroscopic particles (Figure 5 (a)) was higher during the daytime (5:00 - 19:00, $(2.88 \times 10^9) \pm (8.10 \times 10^8)$ #/h) than that at night (from 20:00 to 4:00 the next day, $(2.32 \times 10^9) \pm (2.41 \times 10^8)$ #/h). The peak appeared at noon and the deposition rate reached the top at 12:00 (4.74×10^9 #/h on average). The enhanced deposition rate can be attributed to the strong atmospheric oxidation capacity during the daytime, indicated by OH radical in Figure 5(c), which creates new particles or transfers the pre-existing aerosols to more aged particles through nucleation, semi-volatile partitioning, and multiphase chemistry (Raes et al., 2000; Donahue et al., 2014; Tan et al., 2020; Rudich et al., 2007). For instance, a previous study pointed out that the atmospheric oxidation capacity may enhance the particle formation by oxidizing the trace gases emitted from sources (such as biomass burning) and producing low-volatility condensable vapors, which nucleates in the plume (Wu et al., 2017b). Therefore, the ultrafine particles may be produced during transport (Wu et al., 2017b). During the field campaign, the new particle formation (NPF) events took place frequently (Figure S~~1~~57). Our previous study showed that the NPF events and subsequent growth produced a large amount of hygroscopic and internally mixed particles (Wu et al., 2017b), thus increasing the PNC (as shown in the black line in Figure 5(a)) and leading to the enhanced deposition rate of hygroscopic particles in the day. It is indicated that the deposition rates of particles were mainly influenced by the PNC.

On the contrary, hydrophobic particles (Figure 5(b)) exhibited higher deposition rate at nighttime ($(3.39 \pm 1.34) \times 10^8$ #/h) than that in the day ($(2.58 \times 10^8) \pm (7.60 \times 10^7)$ #/h). The deposition rate of hydrophobic particles peaked at 6:00 - 8:00 during morning rush hours (3.37×10^8 #/h on average), as

indicated by NO, CO, and BC concentrations in Figure 5(c). In the evening, the deposition rate step-wisely increased and reached the maximum (5.17×10^8 #/h on average) at around 21 o'clock. Correspondingly, BC concentrations increased as well. The strong primary emissions (such as the biomass burning process (Wu et al., 2017a)), weak chemical processes, and low boundary layer height (Zhang et al., 2014) resulted in the increased hydrophobic particle number concentration. Thus, people who are exposed to outdoor air during rush hours and the evening may have a higher exposure risk to hydrophobic particles.

It is well-recognized that the freshly emitted hydrophobic particles may be transferred into aged hygroscopic particles (Tan et al., 2020) via atmospheric aging with enhanced volume fractions of inorganic components and organic compounds with higher O:C (Wu et al., 2016; Jimenez et al., 2009). If we take 50 nm-particles as an example, the κ ranged from 0.08 to 0.46 during the entire campaign, implying their different aging degrees. Since BC primarily comes from combustion processes, the κ corresponding to the top 5% highest mass ~~concentrations~~proportion of BC in the hydrophobic particles was employed to represent the κ value of primary emission particles (Figure S~~2~~68). The κ of BC with D_p = 50 nm was ~~0.19 ± 0.10~~0.20 ± 0.12, which was lower than that of the similar size particles during the NPF events ($\kappa = 0.37 \pm 0.03$) in our previous publications (Wu et al., 2017b). In this study, the total DF for adults was ~ 0.258 when κ = ~~0.19~~0.20, while it dropped to ~ 0.217 when κ = 0.37, with a decline change of 15.9%. ~~Assuming particles emitted from different sources (i.e., primary emissions vs. secondary transformation) with the same PNC and diameter, the deposition doses of aged particles in the HRT were lower compared to those of freshly emitted particles.~~

4 Conclusions and Implications

To accurately quantify the effects of both hygroscopicity and external mixing state on the particle deposition, the size-resolved particle hygroscopicity measured at HRT-like conditions (RH = 98%) was used to estimate the deposition doses of submicron particles in the HRT for different age groups with/without considering hygroscopicity using the MPPD model.

The total particle number concentrations were dominated by the hygroscopic particles (number fraction = (91.5 $\pm$ 5.7)%). Taking hygroscopicity into consideration, total deposition doses significantly reduced by about a quarter (24.0% - 24.1%) for all age groups. The greatest reduction took place in doses in the P (25.9% - 26.3%) and TB (24.2% - 26.1%) regions. Head deposition had only minor variations (-0.9% - +0.5%) in both cases. With 270-nm as the boundary, the total doses of smaller particles were overestimated and those of larger particles were underestimated. Regardless of hygroscopicity, the elderly groups received the highest total doses, and children had the lowest doses, which was around half to that for the elderly. Pulmonary doses dominated the deposition pattern. The diurnal variations of deposition rates of hygroscopic and hydrophobic particles were also calculated. The deposition rate of hygroscopic particles was higher during the daytime (2.88×10^9) $\pm$ (8.10×10^8 #/h vs. (2.32×10^9) $\pm$ (2.41×10^8) #/h at night) attributed to the strong atmospheric oxidation capacity. Hydrophobic particles exhibited higher deposition rate at nighttime ((3.39 ± 1.34) $\times 10^8$ #/h) than those in the day ((2.58×10^8) $\pm$ (7.60×10^7) #/h), which was associated with strong primary emissions, weak chemical processes, and

low boundary layer height. The traffic emissions during the rush hours also enhanced the deposition rate of hydrophobic particles. Additionally, fresh emitted particles have lower hygroscopicity and higher DFs compared with ~~aged~~hygroscopic particles with the same diameter and concentration, which may result in higher deposition. Based on a more explicit hygroscopicity measurement at RH = 98%, this work provides an insight into the impact of hygroscopicity on the deposition pattern of submicron particles in the HRT. ~~Moreover, combined with human activities, it deepens the understanding of the relationship of particle mixing state and particle deposition.~~

Although the particle hygroscopicity was measured at a quite high RH (98%), there is still a gap between the measurement conditions and the real HRT-conditions (RH = 99.5%). The higher RH in the lower respiratory tract will lead to greater hygroscopic growth of particles. Since the particle hygroscopicity may reduce the regional and total deposition doses, it is inferred that the higher RH in the lower HRT will further decrease the deposition dose. Therefore, developing the advanced technology for measuring the hygroscopicity in the real HRT-conditions will help to explore the influence of hygroscopicity on the particle deposition in the HRT more accurately.

Due to the limited measurements and physiological parameters, some vital factors which may have effect on the particle deposition in the HRT were not considered in this study, such as gender, the exercise level, and the particle density. Besides, the deposition pattern of particles with diameters larger than 1 μm was not discussed here due to the lack of the measurement of the PNSD and hygroscopicity of coarse particles. While, as an important part of the ambient particle mass, coarse particles may also make a significant contribution to the particle deposition in the HRT (Figure S9). The related research to find out the impact of the particle hygroscopicity on the deposition mass dose of coarse particles ought to be carried out in the future.

Data availability. ~~The data presented in this article can be accessed through the corresponding author Zhijun Wu (zhijunwu@pku.edu.cn).~~The data presented in this article can be accessed on the open accessible research data repository.

Author contribution. ZW, JG, DP, LZ, HH, and AW carried out the field observation and obtained data. RM and TZ processed and analyzed data. All authors discussed the results and contributed to the writing of this paper. RM prepared the manuscript with the contributions of all co-authors. ZW, AV, and MH further modified and improved the manuscript.

Competing interests. The authors declare that they have no conflict of interest.

Acknowledgements. We gratefully acknowledge Applied Research Associates, Inc. (ARA), The Hamner Institutes for Health Sciences, the National Institute of Public Health and the Environment (RIVM), and the Ministry of Housing, Spatial Planning and the Environment for developing and freely distributing the MPPD software.

Financial support. This work was supported by National Natural Science Foundation of China (NSFC,

476   grant no. 42011530121, 91844301) .

477 **References**

478 Asgharian, B., Hofmann, W., and Bergmann, R.: Particle Deposition in a Multiple-Path Model of the
479   Human Lung, Aerosol Sci. Technol., 34, 332-339, 10.1080/02786820119122, 2001.

480 Avino, P., Scungio, M., Stabile, L., Cortellessa, G., Buonanno, G., and Manigrasso, M.: Second-hand
481   aerosol from tobacco and electronic cigarettes: Evaluation of the smoker emission rates and doses
482   and lung cancer risk of passive smokers and vapers, Sci. Total Environ., 642, 137-147,
483   10.1016/j.scitotenv.2018.06.059, 2018.

484 Baltensperger, U.: Urban and rural aerosol characterization of summer smog events during the PIPAPO
485   field campaign in Milan, Italy, J. Geophys. Res., 107, 10.1029/2001jd001292, 2002.

486 Bian, Y. X., Zhao, C. S., Ma, N., Chen, J., and Xu, W. Y.: A study of aerosol liquid water content based
487   on hygroscopicity measurements at high relative humidity in the North China Plain, Atmos. Chem.
488   Phys., 14, 6417-6426, 10.5194/acp-14-6417-2014, 2014.

489 Birmili, W., Stratmann, F., and Wiedensohler, A.: Design of a DMA-based size spectrometer for a large
490   particle size range and stable operation, J. Aerosol Sci., 30, 549-553, 10.1016/S0021-
491   8502(98)00047-0, 1999.

492 Cao, L.: The geographical distribution of normal reference value of lung compliance and total lung
493   capacity. Shaanxi Normal University, Xiʼan, Shaanxi, China, 2009.

494 Chalvatzaki, E. and Lazaridis, M.: A dosimetry model of hygroscopic particle growth in the human
495   respiratory tract, Air Qual., Atmos. Health, 11, 471-482, 10.1007/s11869-018-0555-7, 2018.

496 Chen, S., Wang, H., Lu, K., Zeng, L., Hu, M., and Zhang, Y.: The trend of surface ozone in Beijing from
497   2013 to 2019: Indications of the persisting strong atmospheric oxidation capacity, Atmos. Environ.,
498   242, 10.1016/j.atmosenv.2020.117801, 2020.

499 Chen, Y., Ebenstein, A., Greenstone, M., and Li, H.: Evidence on the impact of sustained exposure to air
500   pollution on life expectancy from China's Huai River policy, Proc. Natl. Acad. Sci. U. S. A., 110,
501   12936-12941, 10.1073/pnas.1300018110, 2013.

502 Ching, J. and Kajino, M.: Aerosol mixing state matters for particles deposition in human respiratory
503   system, Sci. Rep., 8, 8864, 10.1038/s41598-018-27156-z, 2018.

504 Correia, A. W., Pope, C. A., 3rd, Dockery, D. W., Wang, Y., Ezzati, M., and Dominici, F.: Effect of air
505   pollution control on life expectancy in the United States: an analysis of 545 U.S. counties for the
506   period from 2000 to 2007, Epidemiology, 24, 23-31, 10.1097/EDE.0b013e3182770237, 2013.

507 Cuevas-Robles, A., Soltani, N., Keshavarzi, B., Youn, J. S., MacDonald, A. B., and Sorooshian, A.:
508   Hygroscopic and chemical properties of aerosol emissions at a major mining facility in Iran:
509   Implications for respiratory deposition, Atmos. Pollut. Res., 12, 245-254, 10.1016/j.apr.2020.12.015,
510   2021.

511 Duan, X.: Highlights of the Chinese Exposure Factors Handbook (children), China Environment
512   Publishing Group, Beijing, China, 2016.

513 Duan, X., Zhao, X., Wang, B., Chen, Y., Cao S.: Highlights of the Chinese Exposure Factors Handbook
514   (Adults), Science Press, Beijing, China, 2014.

515 Dockery, D. W., Pope, C. A., 3rd, Xu, X., Spengler, J. D., Ware, J. H., Fay, M. E., Ferris, B. G., Jr., and
516   Speizer, F. E.: An association between air pollution and mortality in six U.S. cities, N. Engl. J. Med.,
517   329, 1753-1759, 10.1056/nejm199312093292401, 1993.

518 Donahue, N. M., Robinson, A. L., Trump, E. R., Riipinen, I., and Kroll, J. H.: Volatility and aging of
519   atmospheric organic aerosol, Top. Curr. Chem., 339, 97-143, 10.1007/128_2012_355, 2014.

520 Farkas, A., Furi, P., Then, W., and Salma, I.: Effects of hygroscopic growth of ambient urban aerosol

521   particles on their modelled regional and local deposition in healthy and COPD-compromised human
522   respiratory system, Sci. Total Environ., 806, 10.1016/j.scitotenv.2021.151202, 2022.

523   Ferron, G. A.: The size of soluble aerosol particles as a function of the humidity of the air. Application
524   to the human respiratory tract, J. Aerosol Sci., 8, 251-267, https://doi.org/10.1016/0021-
525   8502(77)90045-3, 1977.

526   Gysel, M., McFiggans, G. B., and Coe, H.: Inversion of tandem differential mobility analyser (TDMA)
527   measurements, J. Aerosol Sci., 40, 134-151, 10.1016/j.jaerosci.2008.07.013, 2009.

528   Haddrell, A. E., Davies, J. F., and Reid, J. P.: Dynamics of Particle Size on Inhalation of Environmental
529   Aerosol and Impact on Deposition Fraction, Environ. Sci. Technol., 49, 14512-14521,
530   10.1021/acs.est.5b01930, 2015.

531   Haritash, A. K. and Kaushik, C. P.: Biodegradation aspects of polycyclic aromatic hydrocarbons (PAHs):
532   a review, J. Hazard. Mater., 169, 1-15, 10.1016/j.jhazmat.2009.03.137, 2009.

533   Hart, M. C., Cook, C. D., and Orzalesi, M. M.: RELATION BETWEEN ANATOMIC RESPIRATORY
534   DEAD SPACE AND BODY SIZE AND LUNG VOLUME, J. Appl. Physiol., 18, 519-&,
535   10.1152/jappl.1963.18.3.519, 1963.

536   Hennig, T., Massling, A., Brechtel, F. J., and Wiedensohler, A.: A Tandem DMA for highly temperature-
537   stabilized hygroscopic particle growth measurements between 90% and 98% relative humidity, J.
538   Aerosol Sci., 36, 1210-1223, 10.1016/j.jaerosci.2005.01.005, 2005.

539   Highwood, E. J. and Kinnersley, R. P.: When smoke gets in our eyes: the multiple impacts of atmospheric
540   black carbon on climate, air quality and health, Environ. Int., 32, 560-566,
541   10.1016/j.envint.2005.12.003, 2006.

542   Hofmann, W.: Modelling inhaled particle deposition in the human lung—A review, J. Aerosol Sci., 42,
543   693-724, 10.1016/j.jaerosci.2011.05.007, 2011.

544   Hu, M., Peng, J., Sun, K., Yue, D., Guo, S., Wiedensohler, A., and Wu, Z.: Estimation of size-resolved
545   ambient particle density based on the measurement of aerosol number, mass, and chemical size
546   distributions in the winter in Beijing, Environ. Sci. Technol., 46, 9941-9947, 10.1021/es204073t,
547   2012.

548   Hussein, T., Saleh, S., dos Santos, V., Boor, B., Koivisto, A., and Löndahl, J.: Regional Inhaled Deposited
549   Dose of Urban Aerosols in an Eastern Mediterranean City, Atmosphere, 10,
550   10.3390/atmos10090530, 2019.

551   Hussein, T., Londahl, J., Paasonen, P., Koivisto, A. J., Petaja, T., Hameri, K., and Kulmala, M.: Modeling
552   regional deposited dose of submicron aerosol particles, Sci. Total Environ., 458-460, 140-149,
553   10.1016/j.scitotenv.2013.04.022, 2013.

554   ICRP (1994) Human respiratory tract model for radiological protection.

555   Jimenez, J. L., Canagaratna, M. R., Donahue, N. M., Prevot, A. S. H., Zhang, Q., Kroll, J. H., DeCarlo,
556   P. F., Allan, J. D., Coe, H., Ng, N. L., Aiken, A. C., Docherty, K. S., Ulbrich, I. M., Grieshop, A. P.,
557   Robinson, A. L., Duplissy, J., Smith, J. D., Wilson, K. R., Lanz, V. A., Hueglin, C., Sun, Y. L., Tian,
558   J., Laaksonen, A., Raatikainen, T., Rautiainen, J., Vaattovaara, P., Ehn, M., Kulmala, M., Tomlinson,
559   J. M., Collins, D. R., Cubison, M. J., Dunlea, E. J., Huffman, J. A., Onasch, T. B., Alfarra, M. R.,
560   Williams, P. I., Bower, K., Kondo, Y., Schneider, J., Drewnick, F., Borrmann, S., Weimer, S.,
561   Demerjian, K., Salcedo, D., Cottrell, L., Griffin, R., Takami, A., Miyoshi, T., Hatakeyama, S.,
562   Shimono, A., Sun, J. Y., Zhang, Y. M., Dzepina, K., Kimmel, J. R., Sueper, D., Jayne, J. T., Herndon,
563   S. C., Trimborn, A. M., Williams, L. R., Wood, E. C., Middlebrook, A. M., Kolb, C. E.,
564   Baltensperger, U., and Worsnop, D. R.: Evolution of Organic Aerosols in the Atmosphere, Science,

326, 1525-1529, 10.1126/science.1180353, 2009.

Khlystov, A., Stanier, C., and Pandis, S. N.: An Algorithm for Combining Electrical Mobility and Aerodynamic Size Distributions Data when Measuring Ambient Aerosol Special Issue ofAerosol Science and Technologyon Findings from the Fine Particulate Matter Supersites Program, Aerosol Sci. Technol., 38, 229-238, 10.1080/02786820390229543, 2004.

Kim, K. H., Jahan, S. A., Kabir, E., and Brown, R. J.: A review of airborne polycyclic aromatic hydrocarbons (PAHs) and their human health effects, Environ. Int., 60, 71-80, 10.1016/j.envint.2013.07.019, 2013.

Kristensson, A., Rissler, J., Londahl, J., Johansson, C., and Swietlicki, E.: Size-Resolved Respiratory Tract Deposition of Sub-Micrometer Aerosol Particles in a Residential Area with Wintertime Wood Combustion, Aerosol Air Qual. Res., 13, 24-35, 10.4209/aaqr.2012.07.0194, 2013.

Li, X., Yan, C., Patterson, R. F., Zhu, Y., Yao, X., Zhu, Y., Ma, S., Qiu, X., Zhu, T., and Zheng, M.: Modeled deposition of fine particles in human airway in Beijing, China, Atmos. Environ., 124, 387-395, 10.1016/j.atmosenv.2015.06.045, 2016.

Liu, P., Song, M., Zhao, T., Gunthe, S. S., Ham, S., He, Y., Qin, Y. M., Gong, Z., Amorim, J. C., Bertram, A. K., and Martin, S. T.: Resolving the mechanisms of hygroscopic growth and cloud condensation nuclei activity for organic particulate matter, Nat. Commun., 9, 4076, 10.1038/s41467-018-06622-2, 2018.

Londahl, J., Massling, A., Pagels, J., Swietlicki, E., Vaclavik, E., and Loft, S.: Size-resolved respiratory-tract deposition of fine and ultrafine hydrophobic and hygroscopic aerosol particles during rest and exercise, Inhal. Toxicol., 19, 109-116, 10.1080/08958370601051677, 2007.

Londahl, J., Massling, A., Swietlicki, E., Brauner, E. V., Ketzel, M., Pagels, J., and Loft, S.: Experimentally Determined Human Respiratory Tract Deposition of Airborne Particles at a Busy Street, Environ. Sci. Technol., 43, 4659-4664, 10.1021/es803029b, 2009.

Lyu, Y., Guo, H., Cheng, T., and Li, X.: Particle Size Distributions of Oxidative Potential of Lung-Deposited Particles: Assessing Contributions from Quinones and Water-Soluble Metals, Environ. Sci. Technol., 52, 6592-6600, 10.1021/acs.est.7b06686, 2018.

Manigrasso, M., Vernale, C., and Avino, P.: Traffic aerosol lobar doses deposited in the human respiratory system, Environ. Sci. Pollut. Res. Int., 24, 13866-13873, 10.1007/s11356-015-5666-1, 2017.

Manigrasso, M., Buonanno, G., Fuoco, F. C., Stabile, L., and Avino, P.: Aerosol deposition doses in the human respiratory tree of electronic cigarette smokers, Environ. Pollut., 196, 257-267, 10.1016/j.envpol.2014.10.013, 2015.

Martonen, T. B. and Schroeter, J. D.: Risk assessment dosimetry model for inhaled particulate matter: I. Human subjects, Toxicol. Lett., 138, 119-132, 10.1016/s0378-4274(02)00411-3, 2003.

Mauderly, J. L. and Chow, J. C.: Health effects of organic aerosols, Inhal. Toxicol., 20, 257-288, 10.1080/08958370701866008, 2008.

MPPD: Multiple-Path Particle Dosimetry Model: https://www.ara.com/mppd/, last access: 2022.

Oberdorster, G.: Pulmonary effects of inhaled ultrafine particles, Int. Arch. Occup. Environ. Health, 74, 1-8, 2001.

Petters, M. D. and Kreidenweis, S. M.: A single parameter representation of hygroscopic growth and cloud condensation nucleus activity, Atmos. Chem. Phys., 7, 1961-1971, 10.5194/acp-7-1961-2007, 2007.

Pope, C. A., 3rd and Dockery, D. W.: Air pollution and life expectancy in China and beyond, Proc. Natl. Acad. Sci. U. S. A., 110, 12861-12862, 10.1073/pnas.1310925110, 2013.

Pope, C. A., III, Ezzati, M., and Dockery, D. W.: Fine-Particulate Air Pollution and Life Expectancy in the United States, N. Engl. J. Med., 360, 376-386, 10.1056/NEJMsa0805646, 2009.

Raes, F., Dingenen, R. V., Vignati, E., Wilson, J., Putaud, J.-P., Seinfeld, J. H., and Adams, P.: Formation and cycling of aerosols in the global troposphere, Atmos. Environ., 34, 4215-4240, https://doi.org/10.1016/S1352-2310(00)00239-9, 2000.

Rajaraman, P. K., Choi, J., Hoffman, E. A., O'Shaughnessy, P. T., Choi, S., Delvadia, R., Babiskin, A., Walenga, R., and Lin, C. L.: Transport and deposition of hygroscopic particles in asthmatic subjects with and without airway narrowing, J. Aerosol Sci., 146, 10.1016/j.jaerosci.2020.105581, 2020.

Rudich, Y., Donahue, N. M., and Mentel, T. F.: Aging of organic aerosol: bridging the gap between laboratory and field studies, Annu. Rev. Phys. Chem., 58, 321-352, 10.1146/annurev.physchem.58.032806.104432, 2007.

Stocks, J. and Quanjer, P. H.: Reference values for residual volume, functional residual capacity and total lung capacity. ATS Workshop on Lung Volume Measurements. Official Statement of The European Respiratory Society, Eur. Respir. J., 8, 492-506, 10.1183/09031936.95.08030492, 1995.

Swietlicki, E., Hansson, H. C., Hameri, K., Svenningsson, B., Massling, A., McFiggans, G., McMurry, P. H., Petaja, T., Tunved, P., Gysel, M., Topping, D., Weingartner, E., Baltensperger, U., Rissler, J., Wiedensohler, A., and Kulmala, M.: Hygroscopic properties of submicrometer atmospheric aerosol particles measured with H-TDMA instruments in various environments - a review, Tellus B, 60, 432-469, 10.1111/j.1600-0889.2008.00350.x, 2008.

Tan, T., Guo, S., Wu, Z., He, L., Huang, X., and Hu, M.: Impact of aging process on atmospheric black carbon aerosol properties and climate effects, Chin. Sci. Bull., 65, 4235-4250, 10.1360/tb-2020-0745, 2020.

Tan, Z., Hofzumahaus, A., Lu, K., Brown, S. S., Holland, F., Huey, L. G., Kiendler-Scharr, A., Li, X., Liu, X., Ma, N., Min, K. E., Rohrer, F., Shao, M., Wahner, A., Wang, Y., Wiedensohler, A., Wu, Y., Wu, Z., Zeng, L., Zhang, Y., and Fuchs, H.: No Evidence for a Significant Impact of Heterogeneous Chemistry on Radical Concentrations in the North China Plain in Summer 2014, Environ. Sci. Technol., 54, 5973-5979, 10.1021/acs.est.0c00525, 2020.

Topping, D. O. and McFiggans, G.: Tight coupling of particle size, number and composition in atmospheric cloud droplet activation, Atmos. Chem. Phys., 12, 3253-3260, 10.5194/acp-12-3253-2012, 2012.

Varghese, S. K. and Gangamma, S.: Particle deposition in human respiratory system: deposition of concentrated hygroscopic aerosols, Inhal. Toxicol., 21, 619-630, 10.1080/08958370802380792, 2009.

Voliotis, A. and Samara, C.: Submicron particle number doses in the human respiratory tract: implications for urban traffic and background environments, Environ. Sci. Pollut. Res. Int., 25, 33724-33735, 10.1007/s11356-018-3253-y, 2018.

Voliotis, A., Bezantakos, S., Besis, A., Shao, Y., and Samara, C.: Mass dose rates of particle-bound organic pollutants in the human respiratory tract: Implications for inhalation exposure and risk estimations, Int. J. Hyg. Environ. Health, 234, 113710, 10.1016/j.ijheh.2021.113710, 2021.

Vu, T., Delgado-Saborit, J., and Harrison, R.: A review of hygroscopic growth factors of submicron aerosols from different sources and its implication for calculation of lung deposition efficiency of ambient aerosols, Air Qual., Atmos. Health, 8, 429-440, 10.1007/s11869-015-0365-0, 2015.

Vu, T. V., Zauli-Sajani, S., Poluzzi, V., and Harrison, R. M.: Factors controlling the lung dose of road traffic-generated sub-micrometre aerosols from outdoor to indoor environments, Air Qual., Atmos.

653   Health, 11, 615-625, 10.1007/s11869-018-0568-2, 2018.

654   Wang, H., Yin, P., Fan, W., Wang, Y., Dong, Z., Deng, Q., and Zhou, M.: Mortality Risk Associated with
655   Short-Term Exposure to Particulate Matter in China: Estimating Error and Implication, Environ.
656   Sci. Technol., 55, 1110-1121, 10.1021/acs.est.0c05095, 2021.

657   Wang, L., Zheng, X., Stevanovic, S., Wu, X., Xiang, Z., Yu, M., and Liu, J.: Characterization particulate
658   matter from several Chinese cooking dishes and implications in health effects, J. Environ. Sci.
659   (China), 72, 98-106, 10.1016/j.jes.2017.12.015, 2018a.

660   Wang, T., Du, Z., Tan, T., Xu, N., Hu, M., Hu, J., and Guo, S.: Measurement of aerosol optical properties
661   and their potential source origin in urban Beijing from 2013-2017, Atmos. Environ., 206, 293-302,
662   10.1016/j.atmosenv.2019.02.049, 2019.

663   Wang, X., Shen, X. J., Sun, J. Y., Zhang, X. Y., Wang, Y. Q., Zhang, Y. M., Wang, P., Xia, C., Qi, X. F.,
664   and Zhong, J. T.: Size-resolved hygroscopic behavior of atmospheric aerosols during heavy aerosol
665   pollution episodes in Beijing in December 2016, Atmos. Environ., 194, 188-197,
666   10.1016/j.atmosenv.2018.09.041, 2018b.

667   Wex, H., Petters, M. D., Carrico, C. M., Hallbauer, E., Massling, A., McMeeking, G. R., Poulain, L., Wu,
668   Z., Kreidenweis, S. M., and Stratmann, F.: Towards closing the gap between hygroscopic growth
669   and activation for secondary organic aerosol: Part 1 – Evidence from measurements, Atmos. Chem.
670   Phys., 9, 3987-3997, 10.5194/acp-9-3987-2009, 2009.

671   Wiedensohler, A., Birmili, W., Nowak, A., Sonntag, A., Weinhold, K., Merkel, M., Wehner, B., Tuch, T.,
672   Pfeifer, S., Fiebig, M., Fjäraa, A. M., Asmi, E., Sellegri, K., Depuy, R., Venzac, H., Villani, P., Laj,
673   P., Aalto, P., Ogren, J. A., Swietlicki, E., Williams, P., Roldin, P., Quincey, P., Hüglin, C., Fierz-
674   Schmidhauser, R., Gysel, M., Weingartner, E., Riccobono, F., Santos, S., Grüning, C., Faloon, K.,
675   Beddows, D., Harrison, R., Monahan, C., Jennings, S. G., O'Dowd, C. D., Marinoni, A., Horn, H.
676   G., Keck, L., Jiang, J., Scheckman, J., McMurry, P. H., Deng, Z., Zhao, C. S., Moerman, M.,
677   Henzing, B., de Leeuw, G., Löschau, G., and Bastian, S.: Mobility particle size spectrometers:
678   harmonization of technical standards and data structure to facilitate high quality long-term
679   observations of atmospheric particle number size distributions, Atmos. Meas. Tech., 5, 657-685,
680   10.5194/amt-5-657-2012, 2012.

681   Wu, Z., Zheng, J., Wang, Y., Shang, D., Du, Z., Zhang, Y., and Hu, M.: Chemical and physical properties
682   of biomass burning aerosols and their CCN activity: A case study in Beijing, China, Sci. Total
683   Environ., 579, 1260-1268, 10.1016/j.scitotenv.2016.11.112, 2017a.

684   Wu, Z. J., Zheng, J., Shang, D. J., Du, Z. F., Wu, Y. S., Zeng, L. M., Wiedensohler, A., and Hu, M.:
685   Particle hygroscopicity and its link to chemical composition in the urban atmosphere of Beijing,
686   China, during summertime, Atmos. Chem. Phys., 16, 1123-1138, 10.5194/acp-16-1123-2016, 2016.

687   Wu, Z. J., Ma, N., Größ, J., Kecorius, S., Lu, K. D., Shang, D. J., Wang, Y., Wu, Y. S., Zeng, L. M., Hu,
688   M., Wiedensohler, A., and Zhang, Y. H.: Thermodynamic properties of nanoparticles during new
689   particle formation events in the atmosphere of North China Plain, Atmos. Res., 188, 55-63,
690   10.1016/j.atmosres.2017.01.007, 2017b.

691   Wu, Z. J., Poulain, L., Henning, S., Dieckmann, K., Birmili, W., Merkel, M., van Pinxteren, D., Spindler,
692   G., Müller, K., Stratmann, F., Herrmann, H., and Wiedensohler, A.: Relating particle hygroscopicity
693   and CCN activity to chemical composition during the HCCT-2010 field campaign, Atmos. Chem.
694   Phys., 13, 7983-7996, 10.5194/acp-13-7983-2013, 2013.

695   Xu, C., Zheng, X., and Shen, S. F.: A numerical study of the effects of ambient temperature and humidity
696   on the particle growth and deposition in the human airway, Environ. Res., 200,

697  10.1016/j.envres.2021.111751, 2021.

698 Youn, J. S., Csavina, J., Rine, K. P., Shingler, T., Taylor, M. P., Saez, A. E., Betterton, E. A., and

699  Sorooshian, A.: Hygroscopic Properties and Respiratory System Deposition Behavior of Particulate

700  Matter Emitted by Mining and Smelting Operations, Environ. Sci. Technol., 50, 11706-11713,

701  10.1021/acs.est.6b03621, 2016.

702 Zhang, Y., Zhang, S., Huang, C., Huang, K., Gong, Y., and Gan, Q.: Diurnal variations of the planetary

703  boundary layer height estimated from intensive radiosonde observations over Yichang, China, Sci.

704  China: Technol. Sci., 57, 2172-2176, 10.1007/s11431-014-5639-5, 2014.

705 Zong, T., Wang, H., Wu, Z., Lu, K., Wang, Y., Zhu, Y., Shang, D., Fang, X., Huang, X., He, L., Ma, N.,

706  Gross, J., Huang, S., Guo, S., Zeng, L., Herrmann, H., Wiedensohler, A., Zhang, Y., and Hu, M.:

707  Particle hygroscopicity inhomogeneity and its impact on reactive uptake, Sci. Total Environ.,

708  151364, 10.1016/j.scitotenv.2021.151364, 2021.

709 Zhu, G.: Physiological constants and psychological status of Chinese population, Peking Union Medical

710  College, Beijing, China, 2006.